




# TOPKi-NBD: a fluorescent small molecule for tumor imaging

Giacomo Pirovano<sup>1</sup> · Sheryl Roberts<sup>1</sup> · Thomas Reiner<sup>1,2,3</sup> 

Received: 14 August 2019 / Accepted: 7 November 2019  
© Springer-Verlag GmbH Germany, part of Springer Nature 2019

## Abstract

**Purpose** OTS514 is a highly specific inhibitor targeting lymphokine-activated killer T cell-originated protein kinase (TOPK). A fluorescently labeled TOPK inhibitor could be used for tumor delineation or intraoperative imaging, potentially improving patient care.

**Methods** Fluorescently labeled OTS514 was obtained by conjugating the fluorescent small molecule NBD to the TOPK inhibitor. HCT116 colorectal cancer cells were used to generate tumors in NSG mice for in vivo studies. Images were generated in vitro using confocal microscopy and ex vivo using an IVIS Spectrum.

**Results** OTS514 was successfully conjugated to a fluorescent sensor and validated in vitro, in vivo, and ex vivo. The labeling reaction led to TOPKi-NBD with 67% yield and 97% purity after purification. We were able to test binding properties of TOPKi-NBD to its target, TOPK, and compared them to the precursor inhibitor. EC<sub>50</sub>s showed similar target affinities for TOPKi-NBD and the unlabeled OTS514. TOPKi-NBD showed specific tumor uptake after systemic administration and was microscopically detectable inside cancer cells ex vivo. Blocking controls performed with an excess of the unlabeled OTS514 confirmed specificity of the compound. Overall, the results represent a first step toward the development of a class of TOPK-specific fluorescent inhibitors for in vivo imaging and tumor delineation.

**Conclusions** TOPK has the potential to be a new molecular target for cancer-specific imaging in a large variety of tumors. This could lead to broad applications in vitro and in vivo.

**Keywords** Molecular imaging · Colorectal cancer · TOPK · Fluorescence · OTS514

## Introduction

Lymphokine-activated killer T cell-originated protein kinase (TOPK), also known as PDZ-binding kinase (PBK), is a mitogen-activated protein kinase-kinase family which has been shown to contribute to the regulation of proliferation

and cell cycle progression [1–3]. High levels of TOPK expression are observed in a significant number of clinical cases of many cancer types, including breast cancer [4], colorectal cancer [5, 6], leukemia and lymphoma [7–9], ovarian cancer [10], lung cancer [11, 12], and glioma [13, 14]. It has been shown that high TOPK levels correlate with poor prognosis due to invasiveness, metastasis, and therapy resistance [10, 11, 15–18]. In cancer, disruption or inhibition of TOPK leads to cytokinesis defects [19], chemosensitization [20], and radiosensitization by altering the G<sub>2</sub>/M checkpoint and increasing apoptosis [21]. TOPK overexpression can lead to transformation in vitro and in vivo [5]. TOPK is also considered to be a stemness ranking signature gene in glioblastoma [22]. Furthermore, human TOPK is not detectable in normal adult tissues apart from testis and placenta [23]. Rodents express TOPK ortholog in the central nervous system and liver. Although the role of TOPK in cancer cells has yet to be fully uncovered, its cancer-specific expression and its known functions make TOPK both an attractive target for drug targeting and a valuable cancer biomarker that can be exploited for molecular imaging [24].

This article is part of the Topical Collection on Preclinical Imaging

**Electronic supplementary material** The online version of this article (<https://doi.org/10.1007/s00259-019-04608-w>) contains supplementary material, which is available to authorized users.

✉ Thomas Reiner  
reinert@mskcc.org

<sup>1</sup> Department of Radiology, Memorial Sloan Kettering Cancer Center, 1275 York Avenue, New York, NY 10065, USA

<sup>2</sup> Department of Radiology, Weill Cornell Medical College, 1300 York Avenue, New York, NY 10065, USA

<sup>3</sup> Chemical Biology Program, Memorial Sloan Kettering Cancer Center, 1275 York Avenue, New York, NY 10065, USA

Based on TOPK expression being higher in tumors compared to surrounding healthy cells, labeled TOPK inhibitors have proven useful for imaging and monitoring malignancies. First-generation drugs have been developed to specifically inhibit TOPK: HI-TOPK-032 (IC<sub>50</sub> of 2  $\mu$ M) [25], OTS514 (IC<sub>50</sub> of 1.5 to 14.0 nM) and OTS964 (IC<sub>50</sub> of 7.6 to 73.0 nM) [26], and ADA-07 [27]. Pantoprazole and ilaprazole, two proton pump inhibitors, have been shown to also target TOPK [28, 29] as have 3-DSC ((2E)-1-(4-Hydroxy-2-methoxyphenyl)-3-(4-hydroxyphenyl)-2-propen-1-one, 3-deoxysappanchalcone) and SKLB-C05 ((R)-1-(4-(1-aminopropan-2-yl) phenyl)-2-hydroxy-4-methylphenanthridin-6(5H)-one hydrochloride) in colorectal cancer [30, 31]. Each of these compounds has been shown to specifically inhibit TOPK over other kinases and/or exhibit TOPK-dependent cell growth inhibition, with promising preclinical results. Aside from OTS514, which has been tested in a Phase I trial in acute myelogenous leukemia, none of these TOPK inhibitors have entered clinical trials. Some attempts are being made to modify TOPK inhibitors for improved pharmacokinetics [32, 33].

We have previously shown that the modification of a TOPK inhibitor with <sup>18</sup>F, a PET isotope, is possible. The obtained molecule, [<sup>18</sup>F]FE-OTS964, was shown to have favorable biodistribution, and its tumor accumulation allowed PET imaging of mice bearing a subcutaneous glioblastoma xenograft [34]. Here, we chose to modify a similar TOPK inhibitor, OTS514, to create a fluorescent tool to target this cancer biomarker. We chose OTS514 due to its reported higher affinity to the target and lower toxicity [26, 35], and validated the fluorescent tracer in a xenograft mouse model of colorectal cancer using HCT116, chosen for its high level of TOPK expression [21].

A fluorescent TOPK inhibitor allows imaging of colorectal cancer in mouse models, with potential for clinical applications.

## Materials and methods

### General

Chemicals were procured from commercial suppliers and used without further purification. (R)-9-(4-(1-aminopropan-2-yl)phenyl)-8-hydroxy-6-methylthieno[2,3-*c*]quinolin-4(5*H*)-one (OTS514) was purchased from Selleck Chemicals (Houston, TX). Water (18.2 M $\Omega$ cm<sup>-1</sup> at 25 °C) was obtained from an Alpha-Q Ultrapure water system from Millipore (Bedford, MA). High-performance liquid chromatography (HPLC) purification and analysis were performed on a Shimadzu UFLC HPLC system with a DGU-20A degasser, an SPD-M20A UV detector, an LC-20AB pump unit, and a CBM-20A communication BUS module. All HPLC purification was carried out on a semi-preparative HPLC (Atlantis® dC18 reverse-phase 5  $\mu$ m silica, 4.6 mm  $\times$  250 mm, column at 1.0 mL/min 5–95% water:acetonitrile 10 min linear gradient, unless otherwise

specified). Liquid chromatography-mass spectrometry (LC-MS) using electrospray ionization (ESI) was performed on Waters instrument with SQD detector for mass identification. A lyophilizer (FreeZone 2.5 Plus, Labconco, Kansas City, MO, USA) was used for freeze drying. <sup>1</sup>H Nuclear magnetic resonance (NMR) and <sup>13</sup>C NMR spectra were recorded on a Bruker AV 600 MHz at the Memorial Sloan-Kettering Nuclear Magnetic Resonance Core Facility. <sup>1</sup>H NMR data are reported as follows: chemical shifts are in parts per million (ppm,  $\delta$ ) relative and are referenced to residual protic peaks. The coupling constants, *J*, are quoted in Hz and its multiplicities by s (singlet), d (doublet), t (triplet), q (quartet), m (multiplet), and br (broadened). <sup>13</sup>C NMR are reported in parts per million relative to the solvent.

All averages are presented as mean  $\pm$  standard deviation. All animal experiments were performed in accordance with protocols approved by the Institutional Animal Care and Use Committee of Memorial Sloan Kettering Cancer Center (MSK) and followed the National Institutes of Health guidelines for animal welfare.

### Synthesis of TOPKi-NBD

TOPKi-NBD: ((R)-8-hydroxy-6-methyl-9-(4-(1-((7-nitrobenzo[*c*][1,2,5]oxadiazol-4-yl)amino)propan-2-yl)phenyl)thieno[2,3-*c*]quinolin-4(5*H*)-one):

4-chloro-7-nitrobenzofuran (9 mg, 1.0 equiv.) was dissolved in 200  $\mu$ g MeOH and NaHCO<sub>3</sub> (11.50 mg, 3.0 equiv.) was added. After the subsequent dropwise addition of (R)-9-(4-(1-aminopropan-2-yl)phenyl)-8-hydroxy-6-methylthieno[2,3-*c*]quinolin-4(5*H*)-one (17 mg, 1.0 equiv.) dissolved in 400  $\mu$ g MeOH, the mixture was stirred for 2 h at room temperature and evaporated under reduced pressure. The resulting residue was purified via HPLC. The purified product, TOPKi-NBD was lyophilized overnight to obtain 65% yield of an orange powder. <sup>1</sup>H NMR(600 MHz, DMSO-*d*<sub>6</sub>)  $\delta$  11.11 (s, 1H, -NH), 8.48 (d, *J* = 8.4 Hz, 1H, -CH<sup>Ar</sup>), 7.83 – 7.74 (m, 3H, Ar-CH(CH<sub>3</sub>)CH<sub>2</sub>-), 7.71 (d, *J* = 5.4 Hz, 1H, -CHCHS), 7.54 – 7.49 (m, 1H, -Ar-NH-), 7.21 – 7.13 (m, 4H, -CH<sup>Ar</sup>), 6.75 (d, *J* = 8.4 Hz, 1H, -CH<sup>Ar</sup>), 5.89 (d, *J* = 5.4 Hz, 1H, -CHCHS), 2.56 (s, 3H, -Ar-CH<sub>3</sub>), 1.07 (d, *J* = 6.3 Hz, 3H, -CH<sub>3</sub>). <sup>13</sup>C NMR (600 MHz, DMSO-*d*<sub>6</sub>)  $\delta$  158.15, 157.46, 153.49, 145.27, 144.68, 143.95, 143.31, 141.57, 135.34, 135.11, 133.67, 133.23, 132.65, 129.92, 128.61, 127.75, 127.25, 127.00, 126.05, 123.20, 117.19, 110.91, 44.45, 37.24, 19.23, 18.41. ESI-MS (ESI<sup>+</sup>), *m/z* calculated for [C<sub>27</sub>H<sub>21</sub>N<sub>5</sub>O<sub>5</sub>S] 527.13 found 528.09 [M + H<sup>+</sup>]. HPLC, *t*<sub>R</sub> = 9.2 min (97%),  $\lambda_{\text{max}}$  absorbance = 475 nm,  $\lambda_{\text{max}}$  emission = 545 nm (420 nm excitation).

### TOPK kinase assay

EC<sub>50</sub> values were determined using an in vitro TOPK kinase assay (TOPK Kinase Enzyme System, Promega #V4094 used

in combination with ADP-Glo™ Assay, Promega #V4095). A serial dilution of the inhibitor was used to test the inhibitor concentration range of 0–40  $\mu\text{M}$  in triplicate. In each well of the 384 low volume plate (Millipore Sigma #CLS3826BC), the following reagents were then added: 2  $\mu\text{L}$  of the substrate (composed of 0.5  $\mu\text{L}$  of MBP Protein (1 mg/mL), 0.025  $\mu\text{L}$  ATP (10  $\mu\text{M}$ ), 1  $\mu\text{L}$  of reaction buffer A supplemented with 50  $\mu\text{M}$  DTT and purified MilliQ water), 2  $\mu\text{L}$  of enzyme (30 ng TOPK (10  $\mu\text{g}/100 \mu\text{L}$ ), and purified MilliQ water). The plate was incubated at room temperature for 120 min. Five microliters per well of ADP-Glo were added and the plate was incubated at room temperature for 40 min. Ten microliters per well of Kinase detection reagent were then added and the plate incubated at room temperature for 30 min before luminescence was detected (integration time 1 s).

## Cell culture

HCT 116 colorectal cancer cells were obtained from UT Texas (Azhdarina Lab) and maintained in 150  $\text{cm}^2$  tissue culture flasks in modified essential medium supplemented with 10% heat-inactivated fetal bovine serum, 100 IU/mL penicillin, and 100  $\mu\text{g}/\text{mL}$  streptomycin. HAP1 cells were purchased by Horizon Discovery (HZGHC000289c017) and were maintained in IMDM media supplemented with 10% heat-inactivated fetal bovine serum. All cells were stored in a cell culture incubator at 37 °C and 5%  $\text{CO}_2$  atmosphere, changing media every 2 days and passaging at 70% confluence. HAP1-WT cells are the progenitor cell line for the CRISPR/Cas9 knockout (TOPK knockout) cell line, HAP1-TOPK k.o. (Supporting Information, Fig. S1a).

## Immunoblotting

Protein lysates were prepared using RIPA lysis buffer (Thermo Scientific, Rockford, IL, USA) with protease inhibitors (Roche, Mannheim, Germany) and phosphatase inhibitors (Sigma). Protein concentration was determined using the BCA assay (Thermo Scientific). Bound antibodies were detected by developing film from nitrocellulose membranes exposed to chemiluminescence reagent (Immobilon Western Chemiluminescent Substrate, EMD Millipore, Merck KGaA, Darmstadt, Germany). The following antibodies were used: anti-TOPK (Sigma SAB5300406 clone 2C8, 1:1000).

## Animal models

To generate mice with HCT116 tumors, 20–24-week-old female athymic nude mice were anaesthetized with 2% isoflurane in 2 L/min medical air.  $1 \times 10^6$  HCT116 cells in 150  $\mu\text{L}$  of 1:1 cell culture media:Matrigel (Corning, Corning, NY) were injected subcutaneously in the right shoulder.

Tumors were allowed to proliferate for 3 weeks, reaching a size of 50–100  $\text{mm}^3$ .

## Imaging and biodistribution

In vitro imaging was performed using HAP1-WT as a TOPK-expressing cell line and HAP1-TOPK k.o. as a negative control (non-TOPK-expressing cell line). Cells were plated, and in the following day, 100 nM TOPKi-NBD agent was added to the media. For blocked cells 200 nM OTS514 was added to each well 30 min prior to TOPKi-NBD. Cells were incubated for 5 h, mounted on a slide using mounting media containing DAPI for nuclear staining and imaged under a confocal microscope.

Ex vivo imaging was performed at 5-h post intravenous injection of 50  $\mu\text{g}/\text{mouse}$  of TOPKi-NBD (Supporting Information, Fig. S1b). For blocking experiments, animals ( $n = 3$ ) were injected with 100  $\mu\text{g}/\text{mouse}$  of unlabeled OTS514 30 min prior to TOPKi-NBD (50  $\mu\text{g}/\text{mouse}$ ). Animals were randomized before injection. Epifluorescence images were obtained with an IVIS Spectrum (PerkinElmer) from excised tumor, muscle, the kidneys, liver, spleen, and blood with a predefined filterset. Autofluorescence was removed through spectral unmixing. Semiquantitative analysis of the TOPKi-NBD signal was conducted by measuring the average radiant efficiency in regions of interest (ROIs) that were drawn on all resected organs under white light guidance. This was measured in  $[\text{p/s}/\text{cm}^2/\text{sr}]/[\mu\text{W}/\text{cm}^2]$ . Tumor and muscle tissues were frozen in OCT immediately after IVIS imaging and sliced (10  $\mu\text{m}$  thickness) in a cryo-microtome (Avantik Cryostatic Microtome). Images were then analyzed under a fluorescence confocal microscope (SP5-Up, MSKCC) and quantified using ImageJ software. All images were modified post-quantification in order to increase brightness/contrast (same brightness/contrast for all images) for better visualization.

## Statistical analysis

All statistical analyses were performed using GraphPad Prism8. Measurements were compared using a *t* test. Statistical significance was considered for *p* values < 0.05 and as follows: ns, not significant, \**p* < 0.05, \*\**p* < 0.01, \*\*\**p* < 0.001.

## Results

### Synthetic production of TOPKi-NBD

TOPKi-NBD was obtained via nucleophilic substitution by fluorescently labeling OTS514 with 4-chloro-7-nitrobenzofuran (Fig. S1c). We confirmed the chemical

identity and purity of all products by HPLC, ESI-MS,  $^1\text{H}$  and  $^{13}\text{C}$  NMR (Supporting Information, Fig. S2 and S3). The synthesis produced TOPKi-NBD in 67% yield. TOPKi-NBD eluted at 9.2 min (5–95% acetonitrile in 10 min) whereas OTS514 eluted 7.1 min on reverse phase HPLC, indicating conversion of the desired product, TOPKi-NBD in good yield. HPLC chromatogram of OTS514 ( $t_R = 7.82$  min), NBD ( $t_R = 14.26$  min), and product, TOPKi-NBD ( $t_R = 9.16$  min), can be seen in Fig. S4. The literature log  $p$  value for NBD was reported to be 1.69 [36]. We have calculated a log  $p$  value of 2.36 for OTS514 and a log  $p$  value of 4.62 for OTS514-NBD (Fig. 1).

### Target affinity of TOPKi-NBD

To demonstrate that the fluorescent conjugation of NBD to OTS514 TOPK inhibitor did not change its affinity for the TOPK target, we performed  $\text{EC}_{50}$  studies. These were obtained using an in vitro TOPK kinase assay (TOPK Kinase Enzyme System, Promega #V4094 used in combination with ADP-Glo<sup>TM</sup> Assay, Promega #V4095). We compared the inhibition potency of unlabeled OTS514 to the fluorescent TOPKi-NBD. These experiments produced similar  $\text{EC}_{50}$ s for both compounds ( $\text{EC}_{50}$  OTS514 =  $0.47 \pm 0.23$   $\mu\text{M}$ ,  $R^2 = 0.94$ ;  $\text{EC}_{50}$  TOPKi-NBD =  $0.49 \pm 0.17$   $\mu\text{M}$ ,  $R^2 = 0.96$ ) (Fig. 2a, b).

### Tumor imaging biodistribution

In order to investigate the imaging potential of TOPKi-NBD, we performed intravenous injection of 50  $\mu\text{g}$  per mouse ( $n = 6$ ) in 200  $\mu\text{L}$  saline. In order to show target specificity of TOPKi-NBD, 3 mice were also pre-injected with 100  $\mu\text{g}$  of unlabeled OTS514 30 min prior to TOPKi-NBD administration. Five hours later, mice were euthanized and the organs (tumor, muscle, kidneys, liver, spleen, and blood) were resected, washed in fresh PBS, and imaged with an IVIS Spectrum imaging system (Fig. 3a). A control cohort was injected with saline ( $n = 6$ ). IVIS imaging showed a clear, cancer-specific accumulation of the probe. This was not visible in the blocked cohort and in the saline control. Brightfield images were used to determine the volume of the organs and select regions of interest around them. The average radiant efficiency was calculated for each organ and plotted (Fig. 3b). Quantification of organ accumulation showed a statistically significant accumulation of TOPKi-NBD in the tumor (average value of  $1.08 \pm 0.27 \times 10^7$  [p/s/cm<sup>2</sup>/sr]/[ $\mu\text{W}/\text{cm}^2$ ]) as compared to blocked and saline control cohorts (respectively  $0.10 \pm 0.05 \times 10^7$  and  $0.28 \pm 0.03 \times 10^7$  [p/s/cm<sup>2</sup>/sr]/[ $\mu\text{W}/\text{cm}^2$ ], \* $p$  value < 0.05). The muscle, kidneys, liver, spleen, and blood levels remained lower than  $0.3 \times 10^7$  for all cohorts, suggesting the cancer specificity of the TOPK-targeting agent TOPKi-NBD.

**Fig. 1** Chemical characterization of TOPKi-NBD. **a** The synthesis of TOPKi-NBD was prepared by conjugating OTS514 with 4-chloro-7-nitrobenzofuran in a one-step reaction. **b** High-performance liquid chromatography (HPLC) of TOPKi-NBD at 280 nm (97% purity) and 420 nm. **c** TOPKi-NBD UV/VIs absorbance and fluorescence spectra (excitation 420 nm) from 400 to 700 nm, 5 nm wavelength resolution. **d** Electrospray positive ionization (ESI+) mass spectra confirm the presence of TOPKi-NBD

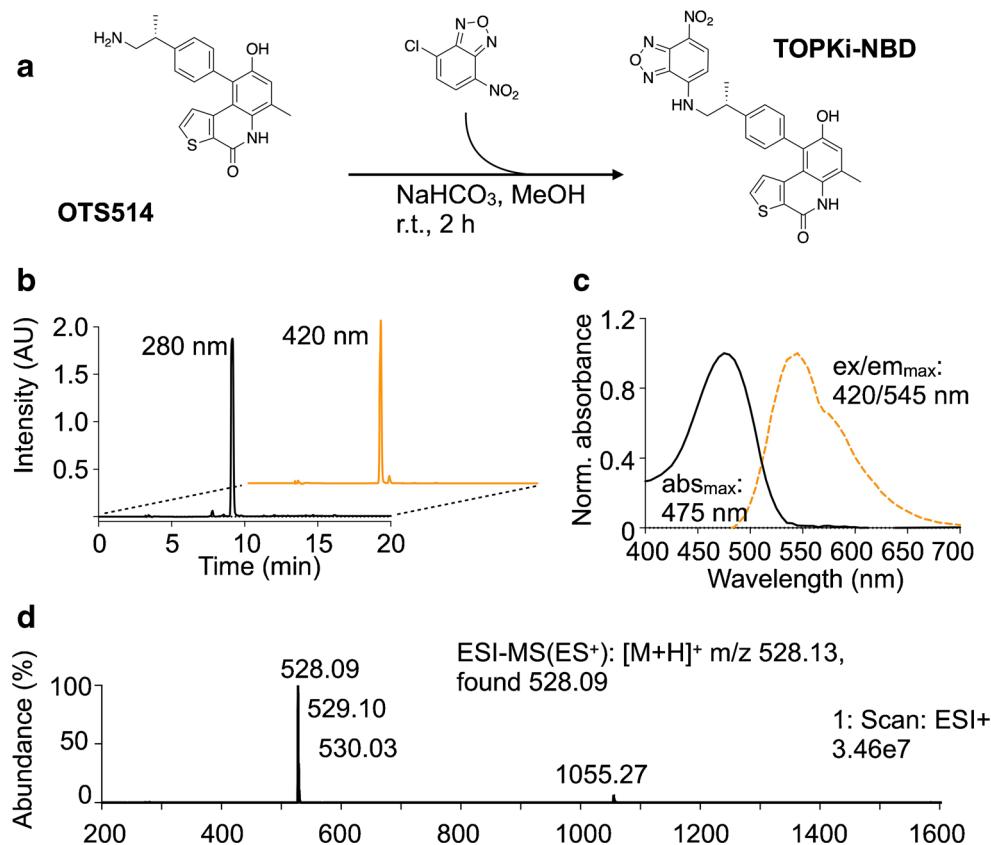
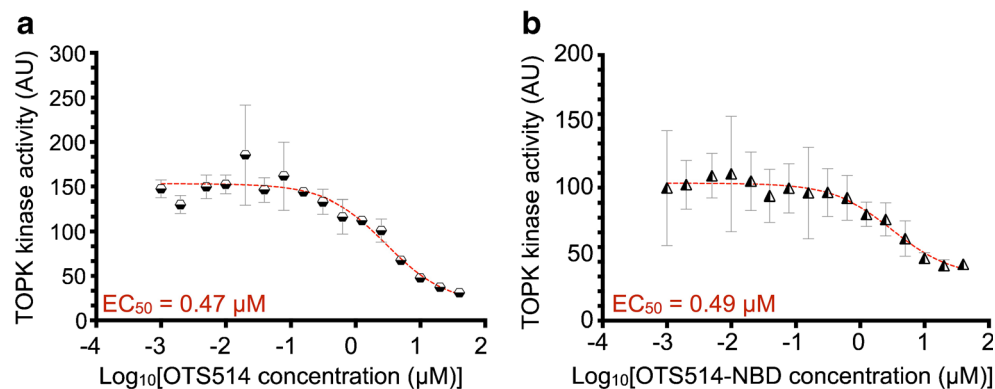




**Fig. 2** TOPK in vitro kinase assay showing specific binding of **a** OTS514 and **b** TOPKi-NBD. Data points represent the average of 3 biological replicates.  $R^2 = 0.763$  for OTS514 and  $R^2 = 0.971$  for TOPKi-NBD



### Microscopy of tumor-specific TOPKi-NBD accumulation

In order to confirm further the imaging potential of TOPKi-NBD, we performed confocal microscopy studies. First, we used adherent HAP1 cells in vitro. A concentration of 100 nM of TOPKi-NBD was added to cells in IMDM media. After 5 h, cells were fixed in 4% paraformaldehyde and imaged. DAPI staining was used to stain nuclei in order to locate the cells, and a fluorescent microscope was used to detect TOPKi-NBD (536 nm). The fluorescent molecule was detectable in HAP1-WT cells and was blockable using 200 nM of unlabeled OTS514 1 h prior to TOPKi-NBD. Saline was also used as negative control to exclude autofluorescence (Fig. S5a). A CRISPR/Cas9 cell line that does not express TOPK, namely HAP1-TOPK k.o., was used as a negative control to exclude unspecific binding of TOPKi-NBD. In HAP1-TOPK k.o. cells, it was not possible to detect bound TOPKi-NBD (Fig. S5b).

TOPKi-NBD was injected in 3 mice per cohort (50 μg/mouse), preceded by 100 μg/mouse of unlabeled OTS514, or saline as control. After 5 h, organs were collected and tumors were split in two parts and frozen in OCT. Frozen sections were obtained (10 μm thickness) and mounted on a coverslip microscope slide for microscopic analysis. NBD

fluorescence emission was visible in microscopy images of tumors from mice injected with TOPKi-NBD ( $n = 3$ ). In blocked animals or saline control cohorts ( $n = 3$  for each cohort), fluorescence was observed to a much lesser degree. Specific cellular uptake was observed by superimposing brightfield and fluorescence images (Fig. 4a). NBD signal was quantified and yielded significantly higher average pixel values for tumors of mice injected with TOPKi-NBD ( $6.62 \pm 4.48$ ) as compared to the two control cohorts (average pixel value of  $0.68 \pm 0.34$  for OTS514/TOPKi-NBD tumor images and  $0.70 \pm 0.22$  for muscle images) (Fig. 4b,  $*p$  value  $< 0.05$ ).

### Discussion

TOPK is a known tumor biomarker with tremendous potential as an imaging agent due to its cancer-specific expression and multifunctional role in cells, including involvement in cancerogenesis, aggressiveness, and as a potential predictor of therapeutic outcome. Here, the versatility of a TOPK inhibitor, OTS514, was used to develop a fluorescent imaging agent targeting TOPK in a preclinical tumor model. We chose a colorectal cancer model due to its reported levels of high TOPK expression [5, 17, 20, 21, 25, 31] (Fig. S1a). The rationale behind choosing NBD as fluorescent dye for

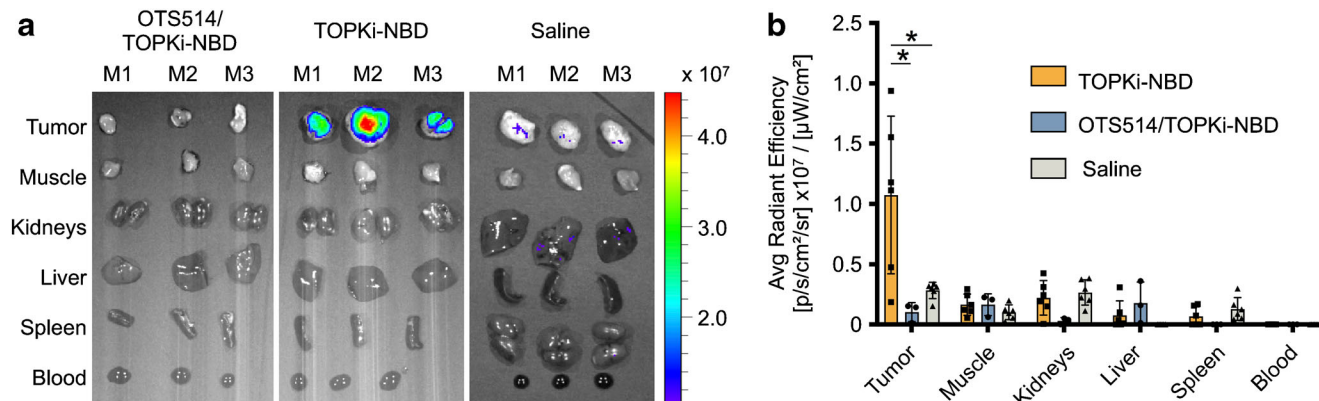


**Fig. 3** TOPKi-NBD biodistribution. **a** Epifluorescence imaging of ex vivo organs post-injection of 50 μg/mouse **b** TOPKi-NBD biodistribution quantification, mean value  $\pm$  SD. Comparison:  $t$  test,  $**p$  value  $< 0.01$

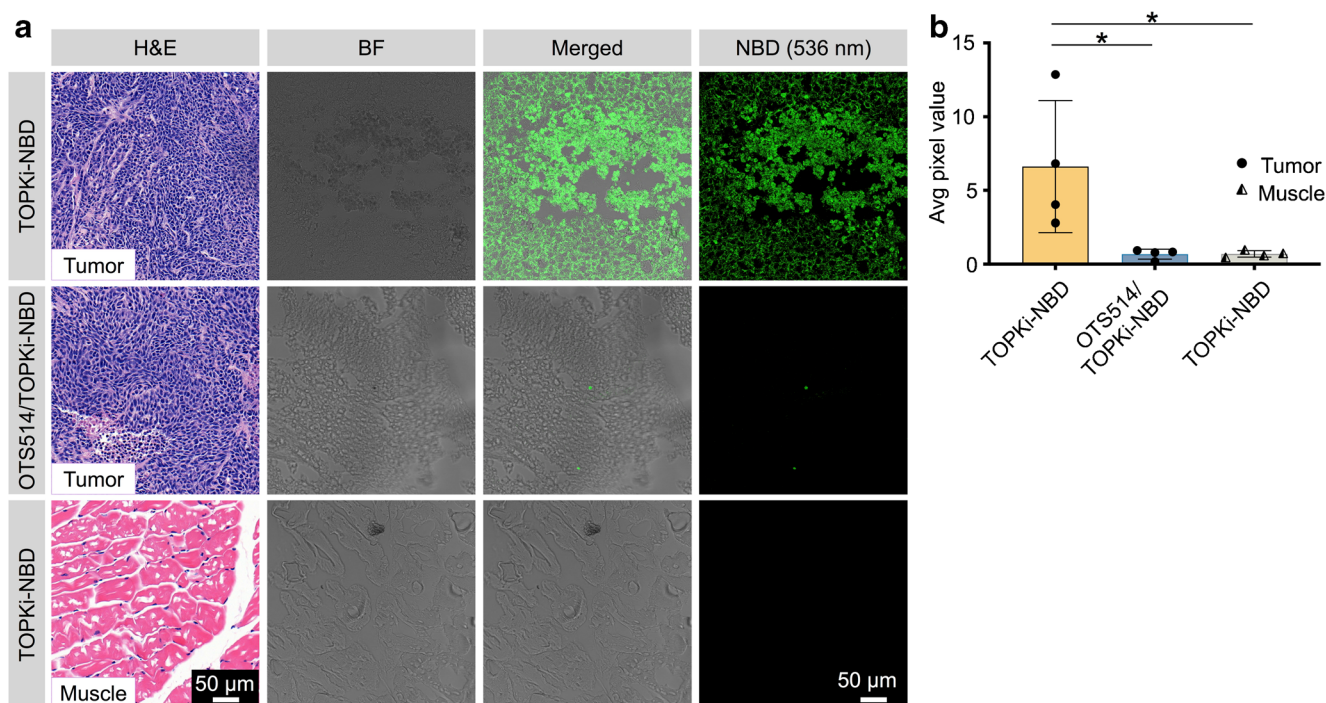


**Fig. 4** Microscopy imaging of ex vivo tissue after TOPKi-NBD injection. **a** Fluorescence microscopy imaging of ex vivo tumor and muscle post-injection of 50  $\mu\text{g}/\text{mouse}$  of TOPKi-NBD, 100  $\mu\text{g}/\text{mouse}$

of unlabeled OTS514 followed by 50  $\mu\text{g}/\text{mouse}$  of TOPKi-NBD for blocking experiment. **b** Quantification of the average pixel value in microscopy images, mean value  $\pm$  SD. Comparison: *t* test, \**p* value < 0.05

conjugation derives from its small footprint, which was considered unlikely to fundamentally perturb OTS514 affinity for TOPK and consequently its ability to penetrate the cellular membrane. This represents a potential limitation due to the low optical penetration quality of the NBD dye as compared to near-infrared dyes, and leaves room for further development. The development of an optical imaging tool in colorectal cancer is considered to be a valuable clinical tool [37–39]. The obtained molecule, TOPKi-NBD, was fully characterized and purified. An in vitro kinase assay was used to assess target affinity of the synthesis product. The  $\text{EC}_{50}$ s thus obtained proved to be similar, confirming the ability of TOPKi-NBD to bind to the target and inhibit its ATP-ADP conversion with an  $\text{EC}_{50}$  of 0.49  $\mu\text{M}$ , as compared to the  $\text{EC}_{50}$  of 0.47  $\mu\text{M}$  of the unlabeled OTS514. It has to be noted that this result is higher than the previously reported median inhibitory concentration of 2.6 nM [26] (patent no. WO/2011/123419). In our study, the inhibitor potency was measured by monitoring the ATP-ADP conversion of commercially available TOPK kinase in vitro. The observed discrepancy might be due to several factors, for example variabilities when comparing an in vitro assay with an in vitro cellular assay [40]. Differences could be based on ATP, kinase, or protein concentrations, as well as other variables within the cellular environment. Another reason for the discrepancy could be off-target effects [35]. The rationale for performing a binding study in the present manuscript was to compare unlabeled OTS514 to the NBD conjugated imaging agent, showing no differences in

binding affinity. In order to confirm the specificity of TOPKi-NBD we performed an in vitro study on HAP1 cells that did express TOPK and on the CRISPR/Cas9 TOPK k.o. of the same cell line. TOPKi-NBD was colocalized within cells expressing TOPK (Fig. S5a), whereas it was not detectable within cells without TOPK targets (Fig. S5b). In vivo, nude mice bearing HCT116 xenografts on their right shoulder were systemically administered TOPKi-NBD. The molecule showed a specific tumor uptake at 5 h post-injection and proved to be blockable with a 2-fold excess dose of OTS514. The used blocking dose was chosen by balancing the target-engagement effect with the toxicity observed from an excessive amount of OTS514 in mice; the results showing a blocking effect with a 2-fold dose of unlabeled compound suggest a slow dissociation from the target. Saline was injected as a control. Pre-administration of a blocking dose reduced tumor uptake significantly, with average radiant efficiencies falling from  $1.075 \pm 0.27 \times 10^7$  [p/s/cm<sup>2</sup>/sr]/[ $\mu\text{W}/\text{cm}^2$ ] in unblocked animals to  $0.10 \pm \times 10^7$  [p/s/cm<sup>2</sup>/sr]/[ $\mu\text{W}/\text{cm}^2$ ] in blocked animals. The same experimental setting was adopted to analyze the images with microscopy and a similar result was obtained (Fig. 4a). TOPKi-NBD was detectable in tumor samples at 5 h post-systemic injection but was not present in tumor cells isolated from mice which received 100  $\mu\text{g}$  of OTS514 prior to TOPKi-NBD injection. Furthermore, muscle tissue was analyzed to interrogate biodistribution and corroborated specificity of the inhibitor. Taken together, these data suggest a favorable tumor-to-

muscle ratio of fluorescent TOPK-targeting agents that can be exploited for cancer imaging and diagnosis. A fluorescent TOPK inhibitor could be used in clinical settings as a margin-delineating tool to facilitate surgery, improving the accuracy and therefore efficacy of the clinical intervention. It is possible to speculate that, thanks to its tumor specificity and its increasingly central role in many mechanisms of cancer biology, TOPK could be an excellent candidate for broad imaging applications.

## Conclusion

In the present study, we produced and characterized TOPKi-NBD, a fluorescent dye targeting TOPK, based on OTS514, a first-generation, selective inhibitor of TOPK. Specific uptake was observed in tumor, with favorable tumor-to-muscle ratios. TOPKi-NBD represents a novel tool for non-invasive detection of this highly promising cancer biomarker. This study is the first step toward the development of a clinically usable fluorescent TOPK inhibitor that could improve clinical intervention and increase survival in a broad spectrum of cancers.

**Acknowledgments** The authors wish to acknowledge the support of Memorial Sloan Kettering Cancer Center's Small Animal Imaging Core Facility, Radiochemistry & Molecular Imaging Probes Core Facility, Integrated Genomics Core Facility, Nuclear Magnetic Resonance Core Facility, Media Preparation Core Facility, and Molecular Cytology Core Facility. We wish to thank Dr. Pat Zanzonico and Ms. Valerie Longo for technical support with IVIS imaging.

**Funding** This work was supported by National Institutes of Health grants R01 CA204441 (T.R.), P30 CA008748, and the Memorial Sloan Kettering Imaging and Radiation Sciences Program (T.R.).

## Compliance with ethical standards

**Conflict of interest** T.R. is shareholder of Summit Biomedical Imaging, LLC and paid consultant for Theragnostics, Inc. G.P. and S.R. declare no conflict of interest.

**Ethical approval (animal work)** All applicable international, national, and/or institutional guidelines for the care and use of animals were followed.

## References

- Abe Y, Matsumoto S, Kito K, Ueda N Cloning and expression of a novel MAPKK-like protein kinase, lymphokine-activated killer T-cell-originated protein kinase, specifically expressed in the testis and activated lymphoid cells. *J Biol Chem*. 2000;275:21525–31.
- Gaudet S, Branton D, Lue RA Characterization of PDZ-binding kinase, a mitotic kinase. *Proc Natl Acad Sci U S A*. 2000;97:5167–72.
- Shinde SR, Gangula NR, Kavela S, Pandey V, Maddika S TOPK and PTEN participate in CHFR mediated mitotic checkpoint. *Cell Signal*. 2013;25:2511–7.
- Park JH, Lin ML, Nishidate T, Nakamura Y, Katagiri T PDZ-binding kinase/T-LAK cell-originated protein kinase, a putative cancer/testis antigen with an oncogenic activity in breast cancer. *Cancer Res*. 2006;66:9186–95.
- Zhu F, Zykova TA, Kang BS, Wang Z, Ebeling MC, Abe Y, et al. Bidirectional signals transduced by TOPK-ERK interaction increase tumorigenesis of HCT116 colorectal cancer cells. *Gastroenterology*. 2007;133:219–31.
- Su TC, Chen CY, Tsai WC, Hsu HT, Yen HH, Sung WW, et al. Cytoplasmic, nuclear, and total PBK/TOPK expression is associated with prognosis in colorectal cancer patients: a retrospective analysis based on immunohistochemistry stain of tissue microarrays. *PLoS One*. 2018;13:e0204866.
- Hu F, Gartenhaus RB, Zhao XF, Fang HB, Minkove S, Poss DE, et al. c-Myc and E2F1 drive PBK/TOPK expression in high-grade malignant lymphomas. *Leuk Res*. 2013;37:447–54.
- Simons-Evelyn M, Bailey-Dell K, Toretsky JA, Ross DD, Fenton R, Kalvakolanu D, et al. PBK/TOPK is a novel mitotic kinase which is upregulated in Burkitt's lymphoma and other highly proliferative malignant cells. *Blood Cells Mol Dis*. 2001;27:825–9.
- Uchida E, Suwa S, Yoshimoto R, Watanabe K, Kasama T, Miura O, et al. TOPK is regulated by PP2A and BCR/ABL in leukemia and enhances cell proliferation. *Int J Oncol*. 2019;54:1785–96.
- Ikeda Y, Park J-H, Miyamoto T, Takamatsu N, Kato T, Iwasa A, et al. T-LAK Cell-Originated Protein Kinase (TOPK) as a Prognostic Factor and a Potential Therapeutic Target in Ovarian Cancer. *Clin Cancer Res*. 2016;22:6110.
- Lei B, Qi W, Zhao Y, Li Y, Liu S, Xu X, et al. PBK/TOPK expression correlates with mutant p53 and affects patients' prognosis and cell proliferation and viability in lung adenocarcinoma. *Hum Pathol*. 2015;46:217–24.
- Shih MC, Chen JY, Wu YC, Jan YH, Yang BM, Lu PJ, et al. TOPK/PBK promotes cell migration via modulation of the PI3K/PTEN/AKT pathway and is associated with poor prognosis in lung cancer. *Oncogene*. 2012;31:2389–400.
- Stangeland B, Mughal AA, Grieg Z, Sandberg CJ, Joel M, Nygård S, et al. Combined expressional analysis, bioinformatics and targeted proteomics identify new potential therapeutic targets in glioblastoma stem cells. *Oncotarget*. 2015;6:26192–215.
- Quan C, Xiao J, Duan Q, Yuan P, Xue P, Lu H, et al. T-lymphokine-activated killer cell-originated protein kinase (TOPK) as a prognostic factor and a potential therapeutic target in glioma. *Oncotarget*. 2018;9:7782–95.
- Brown-Clay JD, Shenoy DN, Timofeeva O, Kallakury BV, Nandi AK, Banerjee PP PBK/TOPK enhances aggressive phenotype in prostate cancer via  $\beta$ -catenin-TCF/LEF-mediated matrix metalloproteinases production and invasion. *Oncotarget*. 2015;6:15594–609.
- Sun H, Zhang L, Shi C, Hu P, Yan W, Wang Z, et al. TOPK is highly expressed in circulating tumor cells, enabling metastasis of prostate cancer. *Oncotarget*. 2015;6:12392–404.
- Zlobec I, Molinari F, Kovac M, Bihl MP, Altermatt HJ, Diebold J, et al. Prognostic and predictive value of TOPK stratified by KRAS and BRAF gene alterations in sporadic, hereditary and metastatic colorectal cancer patients. *Br J Cancer*. 2010;102:151–61.
- Zhang Y, Yang X, Wang R, Zhang X Prognostic value of PDZ-binding kinase/T-LAK cell-originated protein Kinase (PBK/TOPK) in patients with cancer. *J Cancer*. 2019;10:131–7.
- Park JH, Nishidate T, Nakamura Y, Katagiri T Critical roles of T-LAK cell-originated protein kinase in cytokinesis. *Cancer Sci*. 2010;101:403–11.
- Zou J, Kuang W, Hu J, Rao H miR-216b promotes cell growth and enhances chemosensitivity of colorectal cancer by suppressing PDZ-binding kinase. *Biochem Biophys Res Commun*. 2017;488:247–52.



21. Pirovano G, Ashton TM, Herbert KJ, Bryant RJ, Verrill CL, Cerundolo L, et al. TOPK modulates tumour-specific radiosensitivity and correlates with recurrence after prostate radiotherapy. *Br J Cancer*. 2017;117:503–12.
22. Shats I, Gatz ML, Chang JT, Mori S, Wang J, Rich J, et al. Using a stem cell-based signature to guide therapeutic selection in cancer. *Cancer Res*. 2011;71:1772–80.
23. Matsumoto S, Abe Y, Fujibuchi T, Takeuchi T, Kito K, Ueda N, et al. Characterization of a MAPKK-like protein kinase TOPK. *Biochem Biophys Res Commun*. 2004;325:997–1004.
24. Herbert KJ, Ashton TM, Prevo R, Pirovano G, Higgins GS T-LAK cell-originated protein kinase (TOPK): an emerging target for cancer-specific therapeutics. *Cell Death Dis*. 2018;9:1089.
25. Kim DJ, Li Y, Reddy K, Lee MH, Kim MO, Cho YY, et al. Novel TOPK inhibitor HI-TOPK-032 effectively suppresses colon cancer growth. *Cancer Res*. 2012;72:3060–8.
26. Matsuo Y, Park JH, Miyamoto T, Yamamoto S, Hisada S, Alachkar H, et al. TOPK inhibitor induces complete tumor regression in xenograft models of human cancer through inhibition of cytokinesis. *Sci Transl Med*. 2014;6:259ra145.
27. Gao G, Zhang T, Wang Q, Reddy K, Chen H, Yao K, et al. ADA-07 Suppresses solar ultraviolet-induced skin carcinogenesis by directly inhibiting TOPK. *Mol Cancer Ther*. 2017;16:1843–54.
28. Zeng X, Liu L, Zheng M, Sun H, Xiao J, Lu T, et al. Pantoprazole, an FDA-approved proton-pump inhibitor, suppresses colorectal cancer growth by targeting T-cell-originated protein kinase. *Oncotarget*. 2016;7:22460–73.
29. Zheng M, Luan S, Gao S, Cheng L, Hao B, Li J, et al. Proton pump inhibitor ilaprazole suppresses cancer growth by targeting T-cell-originated protein kinase. *Oncotarget*. 2017;8:39143–53.
30. Zhao R, Huang H, Choi BY, Liu X, Zhang M, Zhou S, et al. Cell growth inhibition by 3-deoxysappanchalcone is mediated by directly targeting the TOPK signaling pathway in colon cancer. *Phytomedicine*. 2019;61:152813.
31. Gao T, Hu Q, Hu X, Lei Q, Feng Z, Yu X, et al. Novel selective TOPK inhibitor SKLB-C05 inhibits colorectal carcinoma growth and metastasis. *Cancer Lett*. 2019;445:11–23.
32. Hu Q-F, Gao T-T, Shi Y-J, Lei Q, Liu Z-H, Feng Q, et al. Design, synthesis and biological evaluation of novel 1-phenyl phenanthridin-6(5H)-one derivatives as anti-tumor agents targeting TOPK. *Eur J Med Chem*. 2019;162:407–22.
33. Gilabert-Oriol R, Sutherland BW, Anantha M, Pallaoro A, Bally MB Liposomal OTS964, a TOPK inhibitor: a simple method to estimate OTS964 association with liposomes that relies on enhanced OTS964 fluorescence when bound to albumin. *Drug Deliv Transl Res*. 2019.
34. Pirovano G, Roberts S, Brand C, Donabedian PL, Mason C, de Souza PD, et al. [<sup>18</sup>F]FE-OTS964: a small molecule targeting TOPK for in vivo PET imaging in a glioblastoma xenograft model. *Mol Imaging Biol*. 2019;21:705–12.
35. Lin A, Giuliano CJ, Palladino A, John KM, Abramowicz C, Yuan ML, et al. Off-target toxicity is a common mechanism of action of cancer drugs undergoing clinical trials. *Sci Transl Med*. 2019;11.
36. Bem M, Badea F, Draghici C, Caproiu M, Vasilescu M, Voicescu M, et al. Synthesis and fluorescent properties of new derivatives of 4-amino-7-nitrobenzofurazan. *Arkivoc*. 2007;2007.
37. Feroldi F, Verlaan M, Knaus H, Davidoiu V, Vugts DJ, van Dongen GAMS, et al. High resolution combined molecular and structural optical imaging of colorectal cancer in a xenograft mouse model. *Biomed Opt Express*. 2018;9:6186–204.
38. Kuipers EJ, Grady WM, Lieberman D, Seufferlein T, Sung JJ, Boelens PG, et al. Colorectal cancer. *Nat Rev Dis Primers*. 2015;1:15065.
39. Joshi BP, Wang TD Targeted optical imaging agents in cancer: focus on clinical applications. *Contrast Media Mol Imaging*. 2018;2018:2015237.
40. Cheng Y, Prusoff WH Relationship between the inhibition constant (K<sub>i</sub>) and the concentration of inhibitor which causes 50 per cent inhibition (I<sub>50</sub>) of an enzymatic reaction. *Biochem Pharmacol*. 1973;22:3099–108.

**Publisher's note** Springer Nature remains neutral with regard to jurisdictional claims in published maps and institutional affiliations.